

Can reanalysis datasets describe the persistent temperature and precipitation extremes over China?

Jian Zhu¹ · Dan-Qing Huang^{2,3} · Pei-Wen Yan² · Ying Huang² · Xue-Yuan Kuang²

Received: 26 March 2016 / Accepted: 12 August 2016 / Published online: 29 August 2016
© Springer-Verlag Wien 2016

Abstract The persistent temperature and precipitation extremes may bring damage to the economy and human due to their intensity, duration and areal coverage. Understanding the quality of reanalysis datasets in describing these extreme events is important for detection, attribution and model evaluation. In this study, the performances of two reanalysis datasets [the twentieth century reanalysis (20CR) and Interim ECMWF reanalysis (ERA-Interim)] in reproducing the persistent temperature and precipitation extremes in China are evaluated. For the persistent temperature extremes, the two datasets can better capture the intensity indices than the frequency indices. The increasing/decreasing trend of persistent warm/cold extremes has been reasonably detected by the two datasets, particularly in the northern part of China. The ERA-Interim better reproduces the climatology and tendency of persistent warm extremes, while the 20CR has better skill to depict the persistent cold extremes. For the persistent precipitation extremes, the two datasets have the ability to reproduce the maximum consecutive 5-day precipitation. The two datasets largely underestimate the maximum consecutive dry days over the northern part of China, while overestimate the maximum consecutive wet days over the southern part of

China. For the response of the precipitation extremes against the temperature variations, the ERA-Interim has good ability to depict the relationship among persistent precipitation extremes, local persistent temperature extremes, and global temperature variations over specific regions.

1 Introduction

Persistent climate extremes have a disproportionate impact on ecosystems and society compared to changes in mean climate, due to their intensity, duration, and areal coverage. Different types of persistent extremes, such as heat wave, severe drought, cold spell, are expected to increase in frequency and intensity along with global warming (Liao and Zhang 2013; Sun et al. 2014; Williams et al. 2014; Chen and Zhai 2015). To monitor risk and changes in the persistent temperature and precipitation extremes, several global observation datasets of climate extreme indices based on daily temperature and precipitation have recently been developed (Donat et al. 2013; 2014). However, the datasets based on daily in situ observations are generally with coarse horizontal resolution, lack spatial coverage (Alexander et al. 2006; Donat et al. 2013), as suitable long-term records are sparse for some regions.

By assimilating certain types of observation data into a frozen state-of-the-art analysis/forecast system, the reanalysis dataset has become an important tool of producing observationally constrained data for studying weather and climate variability (Bosilovich et al. 2008; Lin et al. 2014; Huang et al. 2016). Generally, based on operation forecast models, the reanalysis datasets provide complete spatial and temporal coverage of the globe with physically consistent data. Additionally, the reanalysis datasets have their own advantages for detecting the climate extremes. First, the reanalysis data can be a potentially useful source of data for monitoring long-term changes in extremes in

✉ Dan-Qing Huang
huangdq@nju.edu.cn

¹ State Key Laboratory of Hydrology-Water Resources and Hydraulic Engineering, Hohai University, Nanjing 210098, China

² CMA-NJU Joint Laboratory for Climate Prediction Studies, School of Atmospheric Sciences, Nanjing University, Xianlin Avenue No. 163, Nanjing, Jiangsu 210023, People's Republic of China

³ Key Laboratory of Meteorological Disaster of Ministry of Education, Nanjing University of Information Science and Technology, Nanjing 210044, China

data sparse regions. This makes it a popular reference for climate model evaluation (Donat et al. 2014). Second, besides temperature and precipitation variables, the reanalysis datasets also provide the circulation variables. If the reanalysis datasets have good skill for detecting the climate extremes, they may be reliable tools to capture the associated circulations and further discuss the physical mechanisms. Third, the grid data may help solve several issues, including uneven station distribution when calculating averages (Frich et al. 2002), and minimize the impact of data quality issues at individual stations because of averaging (Donat et al. 2013).

However, the reanalysis datasets should not be equated with “observations” and “reality,” due to the systematic biases (e.g., the forecast model, input data, and data assimilation) and uncertainties in the climatological variables. On the global and regional scales, several studies have retrieved different variables from reanalysis datasets to compare the credibility with observations (Smith et al. 2001; Trenberth et al. 2001; Hodges et al. 2011). In China, evaluating the reanalysis datasets is mainly focused on the climatological surface air temperature and precipitation (Zhao and Fu, 2006a, b; Ma et al. 2009; Bao and Zhang 2013; Huang et al. 2016). Although the reanalysis datasets can fairly identify the surface air temperature and precipitation over China, the results are sensitive to the studied time period and regions. For example, the reanalysis datasets (e.g., ERA40, NCEP/NCAR) have good credibility in the surface air temperature in summer, but not in winter (Zhao and Fu 2006a; Ma et al. 2008), particularly for the northern part of China. For the precipitation, the results show that the reasonable identification of the heavy precipitation is still a challenge (Zhao and Fu 2006b; Ma et al. 2009; Huang et al. 2016), particularly for Eastern China and Tibetan Plateau. Most previous studies have focused on the climatology performances of reanalysis datasets based on monthly data. However, climate extremes, including the persistent climate extremes, have received less attention. Recently, You et al. (2013) demonstrated better agreement in single-day temperature extremes between the station data and two widespread used reanalysis (NCEP1 and ERA40) than the persistent temperature extremes.

Particularly, previous studies have analyzed precipitation and temperature extremes separately. However, due to the thermodynamic relations between precipitation and temperature, the two variables are closely linked with each other (Li et al. 2013; Ivancic and Shaw 2016). Associated with background temperature variation, there is evidence that hot temperature and heavy precipitation extremes will become more frequent and extreme in a warmer world (Allan and Soden 2008; O’Gorman and Schneider 2009). It is also indicated that a warm climate is expected to lead to enhance rainfall. This could result in the increase of flooding and the lengthening of dry spells between rainfall events (Ivancic and Shaw 2016). Associated with the local temperature variations, at the inter-annual scale, the relationship between monthly precipitation and air temperature anomaly is generally wet and cool or dry

and hot in most land areas in summer, but wet and warm or dry and cold across high-latitude land areas during winter (Trenberth and Shea 2005). At a short time scale, based on the daily, hourly, and even 5-min station data, several studies indicated a Clausius-Clapeyron (CC) relationship or even super CC relationship between precipitation extremes and temperatures (Lenderink and van Meijgaard 2008; Lenderink and van Meijgaard, 2010; Berg et al. 2013; Westra et al. 2014). Besides the precipitation intensity, Ye et al. (2016) indicated that increasing atmospheric water vapor was directly related to the decreased wet days. Governed by CC relationship (the relationship between temperature and atmospheric water vapor), the extreme temperature may be linked with frequency of wet days. Thus, it is necessary to evaluate the ability of the reanalysis datasets to detect the variation of persistent precipitation extremes response to the temperature variations, including both global temperature and local temperature.

These motivate us to comprehensively evaluate the persistent temperature and precipitation extremes over China calculated from reanalysis datasets against station datasets. The paper is organized as follows: data and methods are described in Section 2. The performances of the reanalysis datasets on the persistent temperature and precipitation extremes are evaluated in Section 3 and Section 4, respectively. Section 5 provides the persistent climate extremes response to the temperature variation, followed by a summary and discussion in Section 6.

2 Data and methods

2.1 Data

Considering four main reasons, we chose two reanalysis datasets in this study, as the twentieth century reanalysis (20CR) (Compo et al. 2011) and Interim European Centre for Medium-Range Weather Forecasts (ECMWF) reanalysis (ERA-Interim) (Dee et al. 2011). First, the two reanalysis datasets have high skills to identify the climatology temperature (including daily mean, maximum and minimum temperature). Second, both reanalysis datasets have variables of mean temperature, maximum temperature, minimum temperature, and precipitation in daily scale, which are needed to calculate the persistent climate extremes. Third, The ERA-Interim, one of the most widespread reanalysis datasets, has good skill to capture the precipitation over East Asia (Huang et al. 2016). Additionally, until recently, the earliest reanalysis product started from 1948, leaving many important climate events such as 1930’s dust bowl droughts uncovered. The 20CR has the longest time serial (1871–) among the popular reanalysis datasets. Thus, the 20CR have the advantage to detect the long-term characteristics of persistent extremes. Table 1 presents detailed information on the two reanalysis datasets. The reanalysis datasets are produced by different numerical weather models and assimilation systems; thus,

Table 1 The characteristics of the two reanalysis datasets

	ERA-Interim	20CR
Atmospheric forecast model	IFS forecasting system	NCEP global forecast system model
Model		
Assimilation algorithm	4DVAR	Ensemble Kalman Filter
Time period	1979-	1871–2012
Horizontal resolution	T255~79 km	T62
Vertical layer	60 levels	28 levels
SST and sea-ice forcing	Daily OISST	HadISST1.1 dataset

they are independent from each other. In order to minimize the impact of resolution, the same horizontal resolution of $2^\circ \times 2^\circ$ covering the period from 1979 to 2011 is chosen for the two reanalysis datasets.

The daily maximum, minimum, mean temperature, and precipitation of 756 stations in China are used (Fig. 1), provided by the National Meteorological Information Center, China Meteorological Administration (<http://data.cma.cn/site/index.html>). Since the climate extremes show significant regional diversities, wide ranging China should be divided into several sub-regions to analyze the regional characteristics. Following the administrative divisions and the characteristics of the monsoon climate of China (Wu and Fu 2013), the following eight sub-regions have been chosen: Northeastern China (I), North China (II), Yangtze-Huaihe River Basin (III), South China (IV), Upper Yellow River (V), Southwestern China (VI), Northwestern China (VII), and Tibetan Plateau (VIII). The details are shown in Fig. 1.

Eleven comprehensively indices of persistent temperature and precipitation are chosen in this study. Referring to You et al. (2013), four persistent temperature extreme frequency

indices are selected, as HWDI, HWFI, CWDI, and CWFI. Referring to Huang et al. (2010), four persistent temperature extreme intensity indices are chosen, as HWDM, HWFM, CWDM, and CWFm. From the ETCCDI list (http://etccdi.pacificclimate.org/list_27_indices.shtml), three persistent precipitation extreme indices are selected, as CDD, CWD, and Rx5d. The detailed descriptions are provided in Table 2.

To represent the background temperature, the surface temperature anomaly dataset (HadCRUT4) on a $5^\circ \times 5^\circ$ grid from the Climate Research Unit (Morice et al. 2012) is used. It contains surface air temperature (from weather stations) over land and sea surface temperature (SST) over ocean (from ship measurements).

The vertically integrated water vapor is calculated as,

$$Q = \frac{1}{g} \int_{P_{top}}^{P_s} q dp, \tag{1}$$

Where P_s is the surface pressure and P_{top} is the pressure at the top of the atmosphere, q is the specific humidity. Here, P_{top} is defined to be 300 hPa, since the specific humidity above 300 hPa is small.

Fig. 1 The distribution of the 756 rain gauge stations used in this study and the eight sub-regions of China: I, Northeastern China (NEC, 42°N – 52°N , 110°E – 135°E); II, North China (NC, 34°N – 42°N , 110°E – 122°E); III, Yangtze-Huaihe River Basin (YHRB, 28°N – 34°N , 110°E – 122°E); IV, South China (SC, 20°N – 28°N , 110°E – 122°E); V, Upper Yellow River (UYR, 34°N – 43°N , 98°E – 110°E); VI, Southwestern China (SWC, 20°N – 34°N , 98°E – 110°E); VII, Northwestern China (NWC, 34°N – 47°N , 74°E – 98°E); VIII, Tibetan Plateau (TP, 27°N – 34°N , 76°E – 98°E)

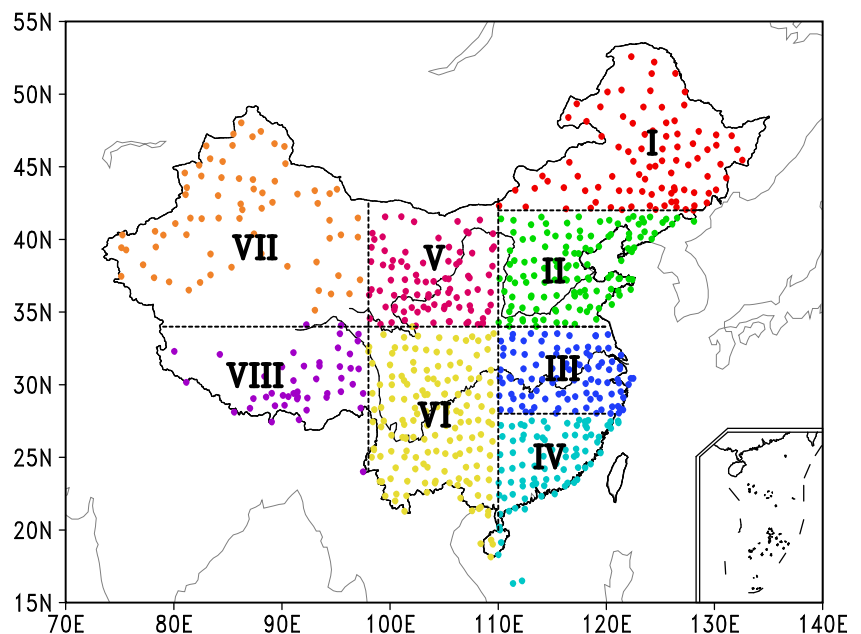


Table 2 The persistent temperature and precipitation extreme indices

ID	Indicator name	Indicator definitions	Units
Persistent warm extreme indices			
HWDI	Heat wave duration index	Annual account number of days when, intervals of at least 6 consecutive days, $TX > T_{norm} + 5$ °C	Days
HWDM	Heat wave duration magnitude	The magnitude of temperature (per day) of the longest heat wave duration event	°C/d
HWFI	Warm spell days index	Annual account number of days when, intervals of at least 6 consecutive days, $TG > 90$ th percentile of 1961–1990	days
HWFM	Warm spell magnitude	The magnitude of temperature (per day) of the longest warm spell event	°C/day
Persistent cold extreme indices			
CWDI	Cold wave duration index	Annual account number of days when, intervals of at least 6 consecutive days, $TN < T_{norm} - 5$ °C	days
CWDM	Cold wave duration magnitude	The magnitude of temperature (per day) of the longest cold wave duration event	°C/day
CWFI	Cold spell days index	Annual account number of days when, intervals of at least 6 consecutive days, $TG < 10$ th percentile of 1961–1990	days
CWFM	Cold spell magnitude	The magnitude of temperature (per day) of the longest cold spell event	°C/day
Persistent precipitation extreme indices			
CDD	Consecutive dry days	Let PR_{ij} be the daily precipitation amount on day i in period j (year). Count the largest number of consecutive days where $PR_{ij} < 1$ mm	Days
CWD	Consecutive wet days	Let PR_{ij} be the daily precipitation amount on day i in period j (year). Count the largest number of consecutive days where $PR_{ij} > 1$ mm	Days
Rx5d	Consecutive 5-day precipitation	Let PR_{kj} be the precipitation amount for the 5-day interval ending k , period j . The maximum 5-day values for period j (year) are as follows: $Rx5d_j = \max (PR_{kj})$	mm/day

Notes: TX daily maximum temperature, TN daily minimum temperature, TG daily mean temperature, $TNorm$ mean of daily minimum temperature for the period of 1961–1990

2.2 Methods

For comparing the extreme indices of station data and the grid data, specifically, the first step is to calculate the extreme indices at each station and each grid point for station data and reanalysis datasets, respectively. Then, the extreme index based on station data is interpolated into a regular grid ($2^\circ \times 2^\circ$ longitude/latitude grid), which is the same as the grid of reanalysis datasets. Finally, the quality of the reanalysis datasets is measured by the pattern correlation coefficient (PCC) and root-mean-square error (RMSE) with reference to the station data, which is calculated by,

$$PCC = \frac{\sum_{i=1}^N (E_{ri} - \overline{E_{ri}}) (E_{si} - \overline{E_{si}})}{\sqrt{\sum_{i=1}^N (E_{ri} - \overline{E_{ri}})^2 \sum_{i=1}^N (E_{si} - \overline{E_{si}})^2}}, \quad (2)$$

$$RMSE = \sqrt{\frac{\sum_{i=1}^n (E_{ri} - E_{si})^2}{n}}, \quad (3)$$

where E_{ri} and E_{si} are the extremes indices in each grid i calculated by reanalysis dataset and station data, respectively. N is the grid number in each region. The PCC (RMSE) reveals the pattern distribution similarity (intensity bias) between the reanalysis dataset and station data. Generally, the reanalysis dataset with large PCC and low RMSE means it has good performance. Additionally, the error between the station data and reanalysis dataset has been measured by the relative differences, which is calculated by,

$$RD = \frac{E_r - E_s}{E_s} \times 100\%, \quad (4)$$

where E_r and E_s are the extreme indices in each grid calculated by reanalysis dataset and station data, respectively.

Trend analysis is performed using the Mann-Kendall test (Mann 1945; Kendall 1975) for monotonic trends to determine if statistically significant trends exist in annual persistent climate extreme. The linear fitting is used to quantitatively diagnose the relationship between precipitation and temperature (Nicholls 2004).

3 Performance of the persistent temperature extremes

3.1 Climatology

The 33-year (1979–2011) mean climatology of the warm extreme indices based on station data and the relative differences between reanalysis dataset and station data are shown in Fig. 2. Station data shows long duration of heat wave over the middle and northern part of China, but shows short duration over the eastern part of China (Fig. 2a). Differences between the two reanalysis datasets and station data show that the 20CR has ability to capture the feature of the heat wave duration, with a little discrepancy over northeastern China (Fig. 2b). The ERA-Interim, by contrast, has largely overestimated (underestimated) the heat wave duration over the northwestern part of China (the southern part of China and Tibetan Plateau) (Fig. 2c). In comparison of the PCC and RMSE, the 20CR has high skill in reproducing the climatological HWDI. The HWFI index, named as a percentile index, indicates the persistent warm spell day. The station data shows shorter duration of warm spell over the eastern part of China, while the duration is longer over the western part of China (Fig. 2d). Combined with the results of PCC and RMSE, the two reanalysis datasets have poor abilities (Fig. 2e, f) in reproducing HWFI, particularly for the western part of China. For the intensity indices (Fig. 2g, j), the HWDM and HWFM have gradually decreased from the southeastern to the northwestern part of China. This is quite similar to the distribution of climatological temperature. Different from the performance of the frequency indices, both the two reanalysis datasets have better ability to capture the intensity indices, particularly the ERA-Interim (the PCC ≥ 0.33 and the RMSE ≤ 9). It should be noticed that both reanalysis datasets underestimate the intensity indices over the western part of China (Fig. 2h, i, k, l).

The climatology mean (1979–2011) of the cold extremes indices based on station data and the differences ratio between reanalysis datasets and station data are shown in Fig. 3. For the two frequency indices of CWDI and CWFI, station data shows quite homogeneous distribution over China (Fig. 3a, d). As shown in the relative differences, both reanalysis datasets have overestimated the cold wave duration over the western part of China (Fig. 3b, c). Moreover, the ERA-Interim has underestimated the cold wave duration over Northeastern China (Fig. 3c). Large discrepancies are also indicated in the CWFI differences between the two reanalysis datasets and station data (Fig. 3e, f). In comparison of the PCC and RMSE, two reanalysis datasets have poor abilities to capture the two frequency indices. For the intensity indices (Fig. 3g, j), station data shows that the CWDM and CWFM have gradually decreased from southeast to northwest over China. The two reanalysis datasets have better ability to capture the intensity indices than the frequency indices. To sum up, for the

climatological persistent temperature indices, the two reanalysis datasets have the ability to capture the intensity indices. However, the persistence in frequency is poorly identified by the two reanalysis datasets. Also, the two reanalysis datasets exhibit large discrepancies for all indices over the western part of China (west to 95° E). Since the western part of China includes a huge terrain (Tibetan Plateau), how to well represent the persistent climate extremes over there is still an open issue.

3.2 Temporal variations

In this section, we evaluated the ability of two reanalysis datasets to identify the year-to-year variations and trends. The reanalysis dataset with good performance (temporal correlation higher than 0.35 and small RMSE) has been chosen. Taking the HWFI as an example, Fig. 4 shows the time serials of regional-mean HWFI over the 7 sub-regions in 1979–2011. In comparison of the PCC and RMSE, the ERA-Interim has good ability to capture temporal variation of HWFI in most regions, except Northwestern China. For other indices, the reanalysis dataset of good performance and the sub-regions are summarized in Table 3. Overall, the ERA-Interim has high skill to identify the temporal variation of warm persistent extremes, particularly in North China, Northeastern China, Yangtze-Huaihe River Basin and Upper Yangtze Basin, while the 20CR has quite good ability to capture the year-to-year variation of the cold persistent extremes indices over the western part of China. This result is also in agreement with the performance of the climatological extreme indices.

In the period of 1979–2011, the HWDI and HWFI significantly increase over most parts of China, particularly over the northern part of China (Fig. 5a, d). In comparison, the ERA-Interim has better ability in reproducing the tendency of HWDI and HWFI than the 20CR (Fig. 5b–f). It should be noticed that there is still some inconsistency in the western China. For the frequency indices of cold extremes, CWDI and CWFI weakly increase over the middle parts of China, while decrease over the other regions (Fig. 5g, j). The 20CR has the ability to capture this increasing tendency (Fig. 5h, k). The two reanalysis datasets have overestimated the decreasing tendencies over the western part of China. In comparison, the 20CR has better ability to capture the significant trend of CWFI, particularly over the Northwestern China. Quite consistent distribution lies in the tendency of HWDM and HWFM: significant increasing trends cover most regions (Fig. 5m, p). The two reanalysis datasets have the ability to detect the increasing tendency, but overestimate the intensity (Fig. 5n–r). However, the two reanalysis datasets have quite a poor ability to detect the tendencies of CWDM and CWFM (Fig. 5s–x).

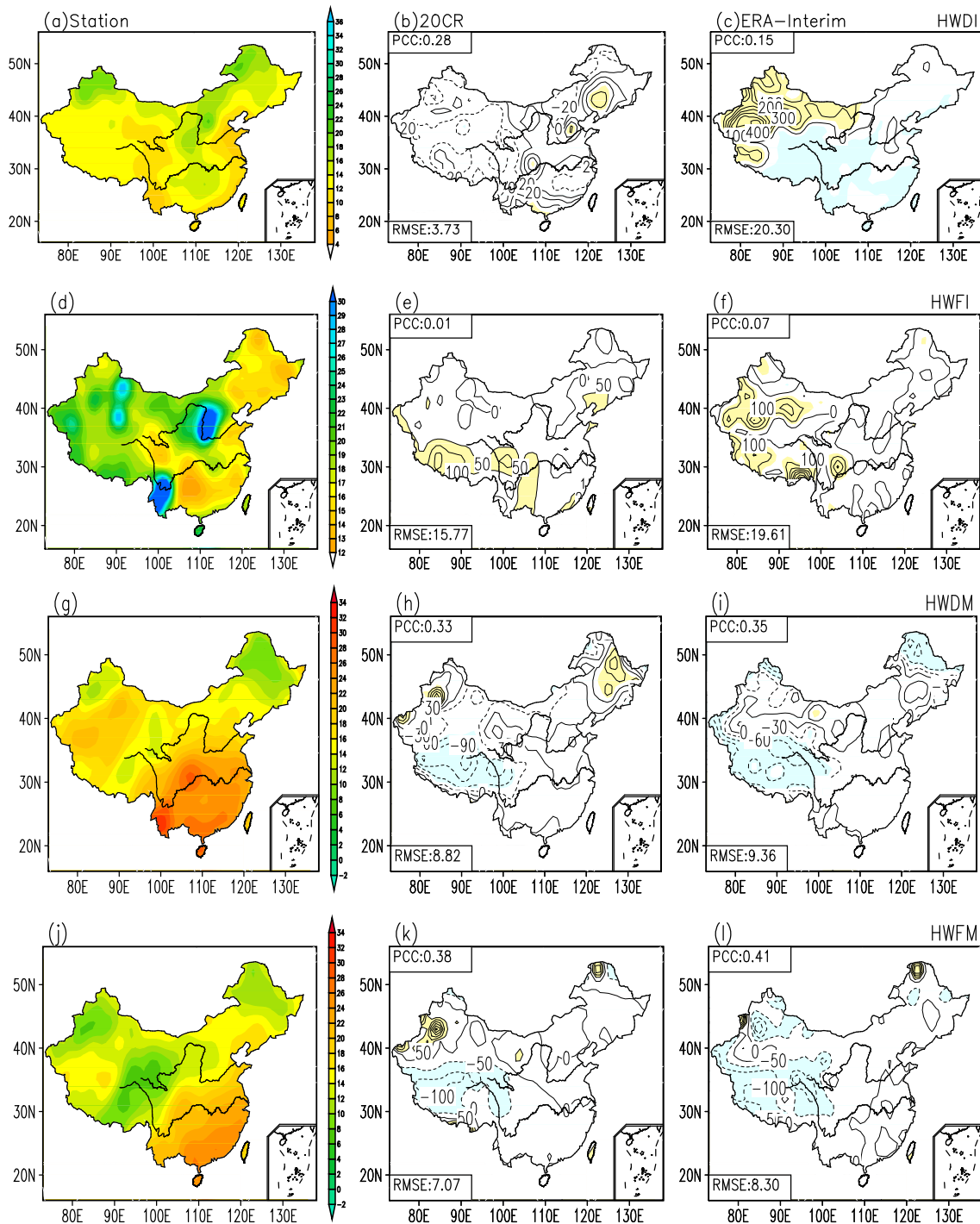


Fig. 2 The climatological annual mean (1979–2011) of warm extreme indices (HWDI: **a–c**, HWFI: **d–f**, HWDM: **g–i**, HWFM: **j–l**) in station data (the *left column*) and the relative differences between the 20CR (the *middle column*), ERA-Interim (the *right column*) and the station data. The

PCCs and RMSEs of each reanalysis dataset are shown in the upper-left and lower-left corner, respectively (the *middle and right columns*). The values $\geq 50\%$ and $\leq -50\%$ have been shaded in the *middle and right column figures*

4 Performance of the persistent precipitation extreme

The climatological mean (1979–2011) of CDD is shown in Fig. 6. The station data indicates long (short) duration of dry day lies in the northern part of China (middle reach of Yangtze River). Two reanalysis datasets can

capture the CDD over the eastern part of China, particularly for the ERA-Interim. However, in the northern part of China (100° – 135° E, 37.5° – 55° N, red box in Fig. 6), two reanalysis datasets have largely underestimated the CDD. The uncertainty may remind us to further discuss the possible reasons. On one hand,

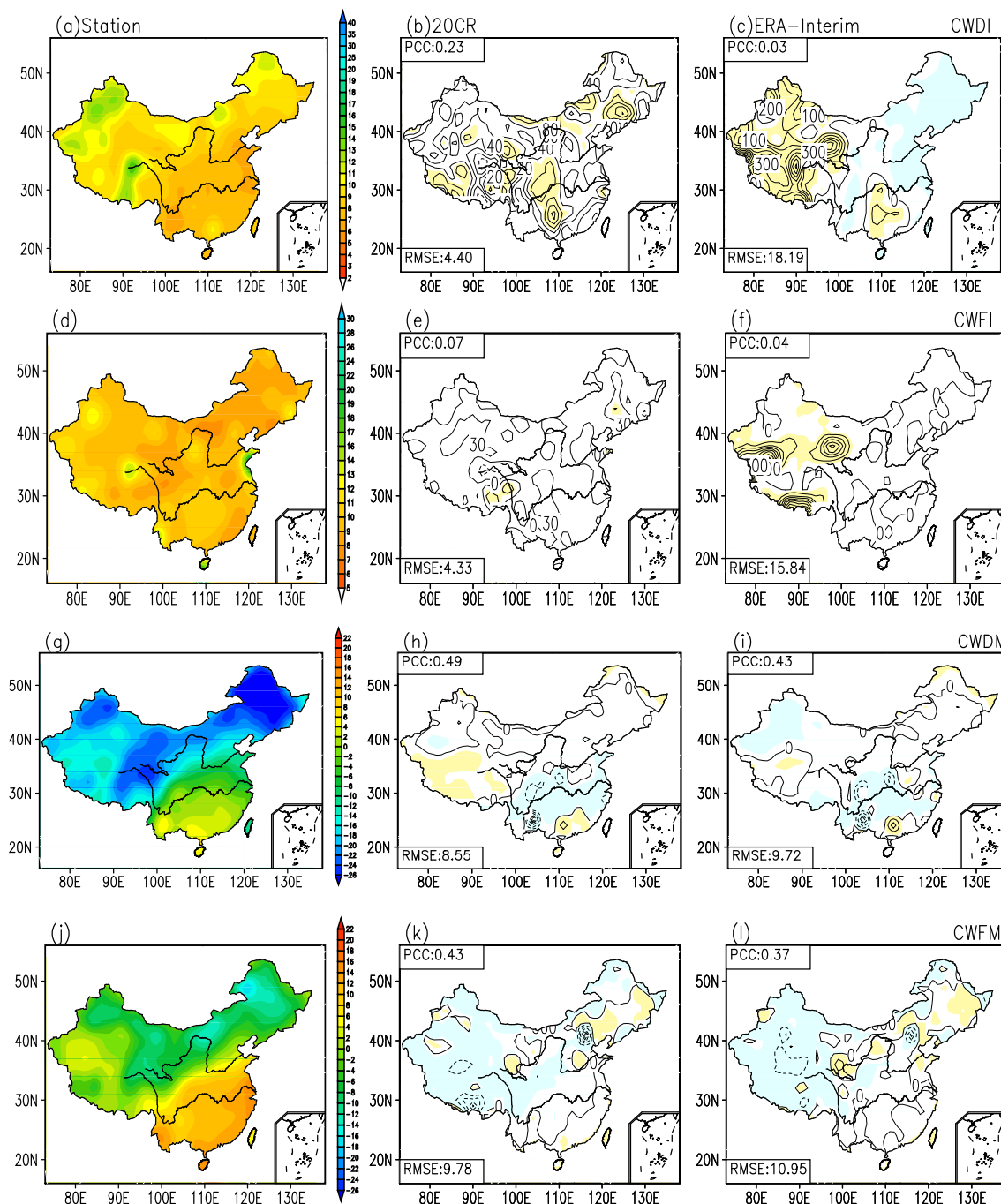


Fig. 3 Same as Fig. 2, but for the climatological annual mean (1979–2011) of cold extreme indices (CWDI: a–c, CWFI: d–f, CWDM: g–i, CWFM: j–l)

what we are not concerned is that whether the occurrence season of CDD from reanalysis dataset is in consistent with that of station data. The station data indicates that maximum consecutive dry day occurs in autumn (purple color) over Southeastern China, while it frequently occurs in winter (green color) over the central China (Fig. 7a). Over the northern part of China, the dry day persistently occurs in spring and winter. The two reanalysis datasets can capture the occurrence season (autumn) of CDD over the eastern part of China. However, for the

northern part of China, the two reanalysis datasets detect that winter is the only occurrence season. This is not consistent with station data, which may be one of the possible reasons for the large discrepancies over the northern part of China. On the other hand, we further compare the numbers of dry days (daily precipitation <1 mm) in the two reanalysis datasets during the occurrence season (from January to May) (Fig. 7d–f). Clearly, the ERA-Interim has good skill to capture the numbers of dry days during winter to spring (Fig. 7f). However,

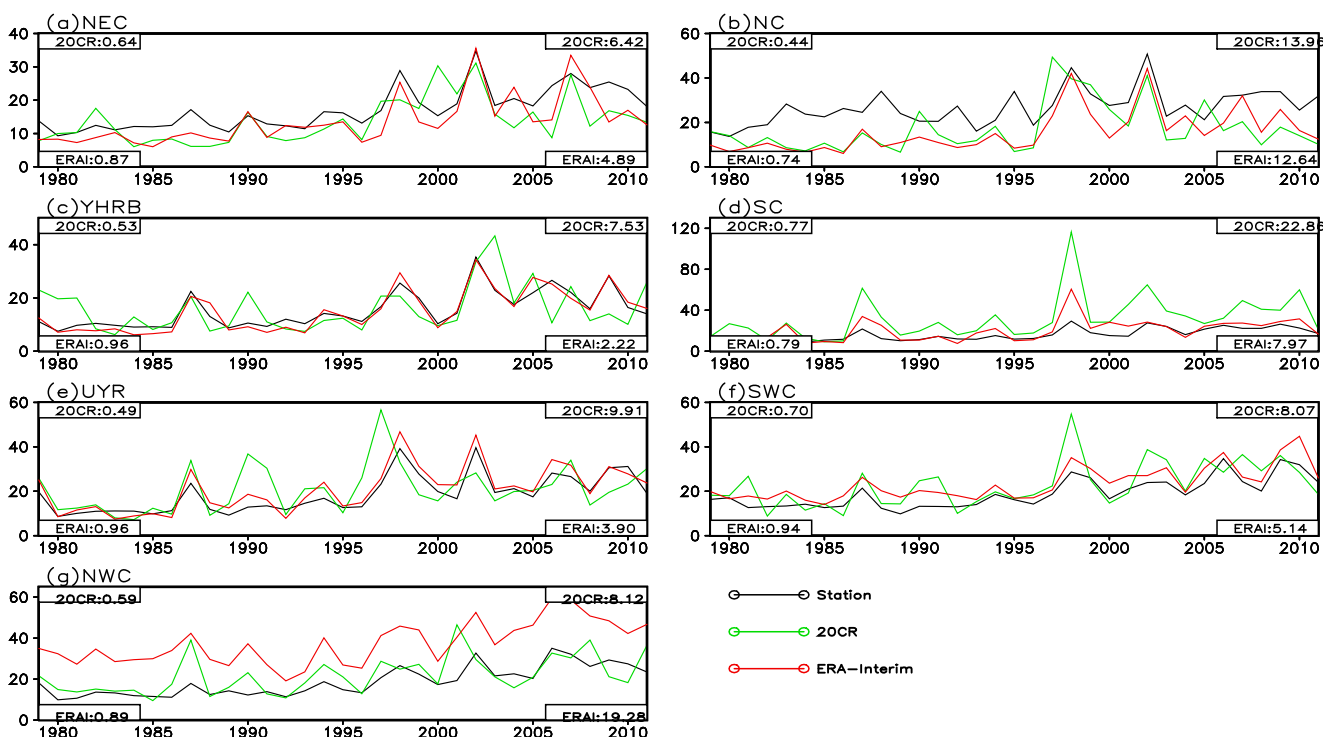


Fig. 4 Time series of the HWFI over seven sub-regions in 1979–2011. The temporal correlations (*left corner*) and RMSEs (*right corner*) of 20CR and ERA-Interim are shown in the *upper-left* and *lower-left* corner, respectively

the 20CR underestimates the dry days over most parts of China, particularly over the southern and the northern part of China (Fig. 7e). This may be associated with the underestimation of CDD over North China.

Figure 8 shows the climatological mean CWD. The CWD of station data decreases from the southeastern to the northwestern part of China (Fig. 8a). The two

reanalysis datasets have the ability to capture this pattern (Fig. 8a–b), with highest consistency over Northwestern China. However, they largely overestimate the maximum consecutive rain days over the southern part of China (red boxes in Fig. 8). To detect the possible reasons, the occurrence season of CWD and the numbers of rain days are compared. In the station data (Fig. 9a), the maximum

Table 3 The sub-regions with good performance of the reanalysis datasets in reproducing the temporal variations of persistent temperature and precipitation extremes (the temporal correlation coefficients are given in the parentheses)

Indices	ERA-Interim	20CR
HWDI	NEC (0.81), NC (0.84), YHRB (0.86), SC (0.87)	UYB (0.64), SC (0.72), SWC (0.6)
HWDM	NEC (0.78), NC (0.82), YHRB (0.69), UYB (0.75), NWC (0.74)	
HWFI	NEC (0.87), NC (0.74), YHRB (0.96), SC (0.79), UYB (0.96), SWC (0.94)	
HWFM	NEC (0.73), NC (0.86), YHRB (0.93), UYB (0.94), SWC (0.71), NWC (0.81), SC (0.67)	
CWDI	NEC (0.45), YHRB (0.65), UYB (0.45)	SWC (0.61), NWC (0.46)
CWDM	NC (0.61), UYB (0.35), NWC (0.44)	NEC (0.49)
CWFI	YHRB (0.62), SC (0.69), SWC (0.51)	NWC (0.65), NC (0.5), UYB (0.38)
CWFM	NC (0.84), YHRB (0.77), UYB (0.7), SWC (0.69), NWC (0.57)	NEC (0.65), SC (0.54)
CDD	NEC (0.52), NC (0.76), YHRB (0.71), SC (0.47), SWC (0.43)	
CWD	NEC (0.54), UYB (0.51), NWC (0.44)	
Rx5d	NEC (0.76), NC (0.64), YHRB (0.84), SC (0.4), UYB (0.6), NWC (0.44)	

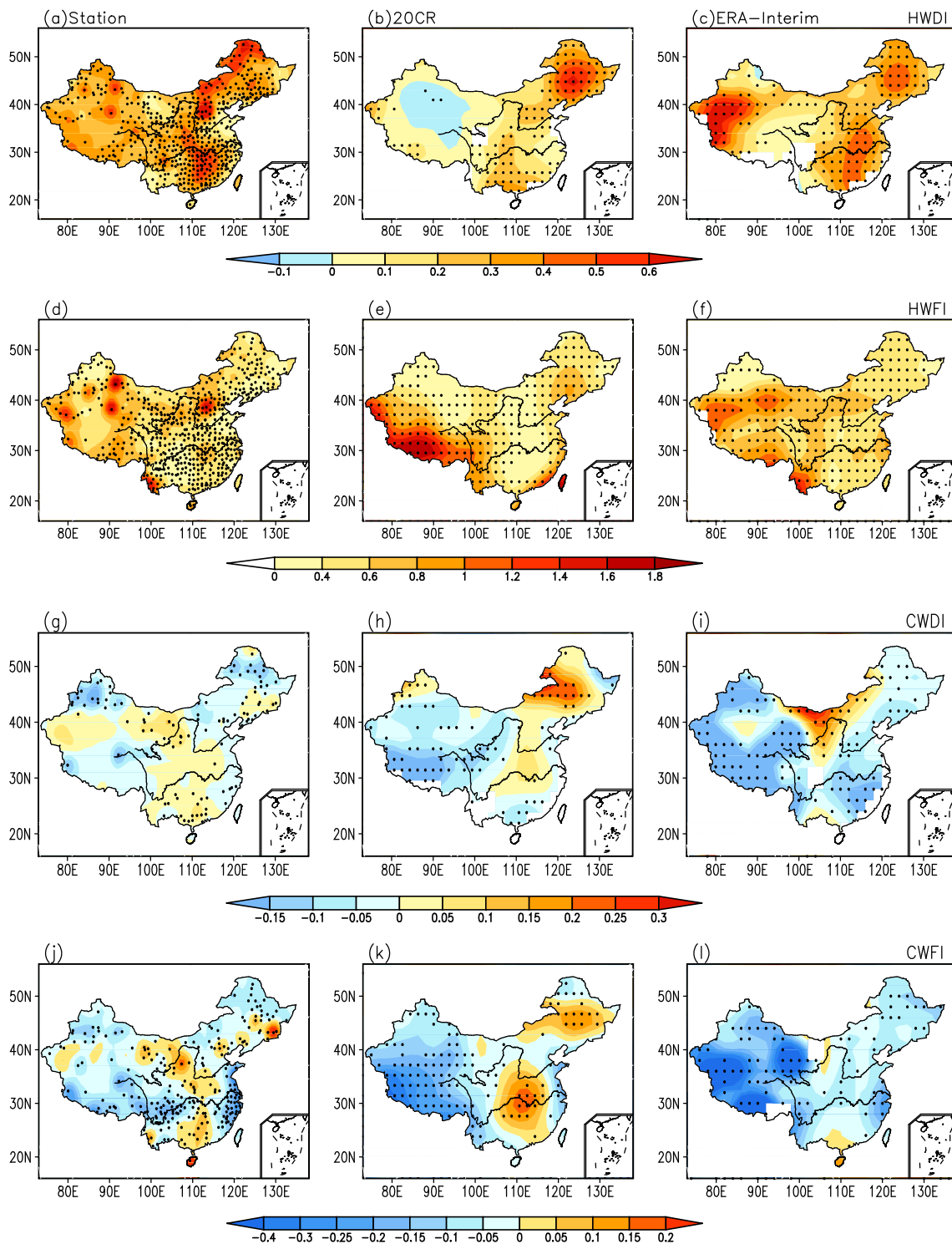


Fig. 5 The trends of HWDI (a–c), HWFI (d–f), CWDI (g–i), CWFI (j–l), HWDM (m–o), HWFM (p–r), CWDM (s–u), CWFM (v–x) in station data (the first column), 20CR (the second column) and ERA-Interim (the

third column) in 1979–2011. Values with magnitude significant at the 90 % confidence level are marked in black dots

consecutive rain day occurs in summer over Northeastern China, while it occurs in autumn in the middle part of China. In the southern part of China, the maximum consecutive rain day easily occurs in spring and summer

over the eastern and the western part of China, respectively. The two reanalysis datasets cannot capture the occurrence season. This may be associated with the large biased lies in depicting the CWD from the two

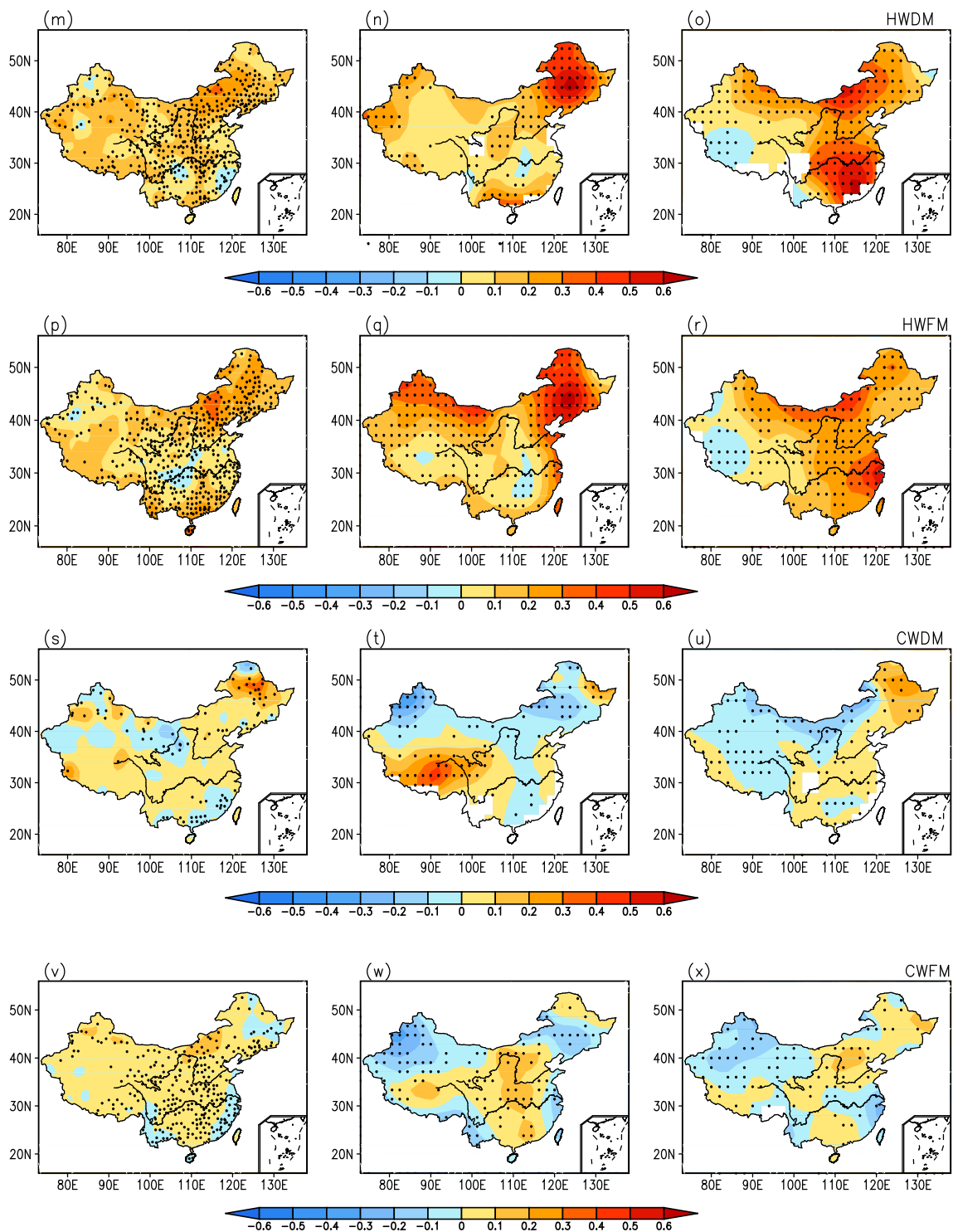


Fig. 5 continued.

reanalysis datasets. Secondly, the numbers of rain days (daily precipitation >1 mm) in the occurrence season (from March to August) are shown in Fig. 9d–f. Clearly, the two reanalysis datasets largely overestimate the numbers of rain days over the southern part of China, particularly for the 20CR. This may be another possible reason

for the overestimation of CWD over the southern part of China. Thus, we may infer that the discrepancies of CWD and CDD between station data and the reanalysis dataset may be due to the incorrectly identification of occurrence season, or the unreal numbers of dry days/rain days detected by reanalysis datasets.

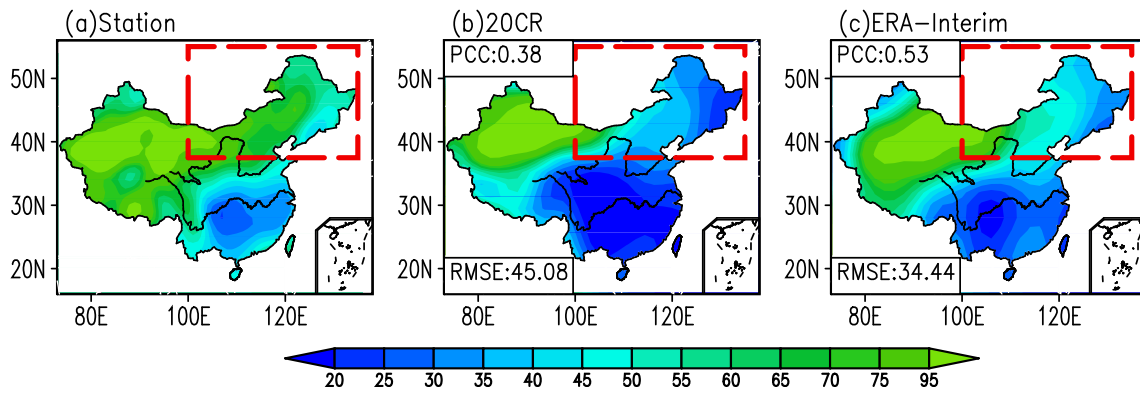


Fig. 6 The climatological annual mean (1979–2011) of CDD in station data (a), 20CR (b) and ERA-Interim (c). The PCCs and RMSEs of each reanalysis dataset are shown in the upper-left and lower-left corner,

respectively, in (b) and (c). The red dashed boxes indicate the northern part of China (100°–135° E, 37.5°–55° N)

Figure 10 shows the climatological mean Rx5d. In the station data, the Rx5d gradually decreases from the southeastern to the northwestern part of China (Fig. 10a). The two reanalysis datasets can capture this decreasing pattern (Fig. 10a–b), with highest consistency over Northwestern China. The difference is that the 20CR has better ability to capture the intensity, while

the ERA-Interim has better ability to capture the spatial distribution.

For the year-to-year variation of the three persistent precipitation indices, the performance of the two reanalysis datasets has been summarized in Table 3. It shows that the ERA-Interim has better ability to capture variation of CDD, CWD and Rx5d than the 20CR, particularly over the eastern part of China (not shown).

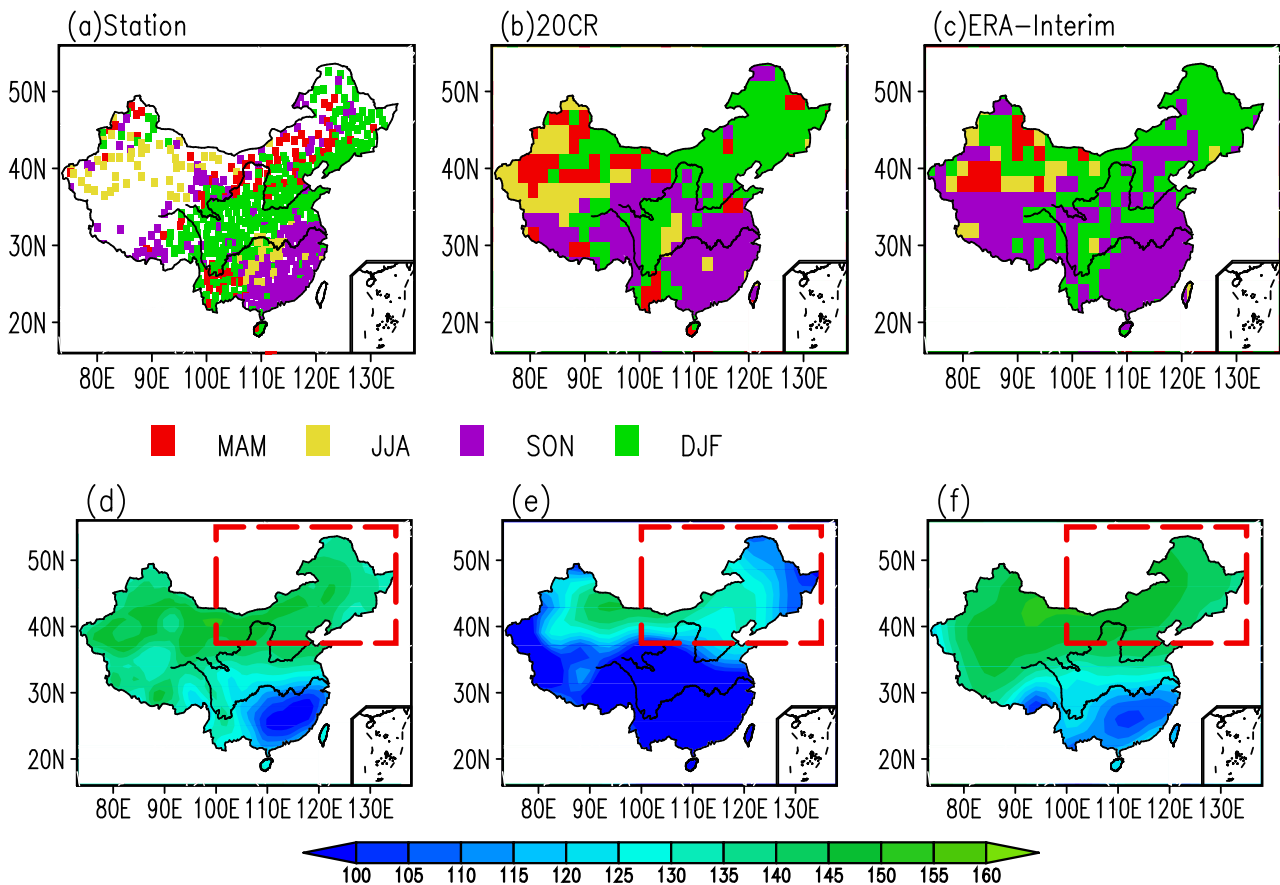


Fig. 7 The climatological (1979–2011) occurrence season of CDD (a–c) and the numbers of dry days during winter and spring (d–f) in station data (the left column), 20CR (the middle column) and ERA-Interim (the right

column). The red dashed boxes in Figs. 7d–f indicate the northern part of China (100°–135° E, 37.5°–55° N)

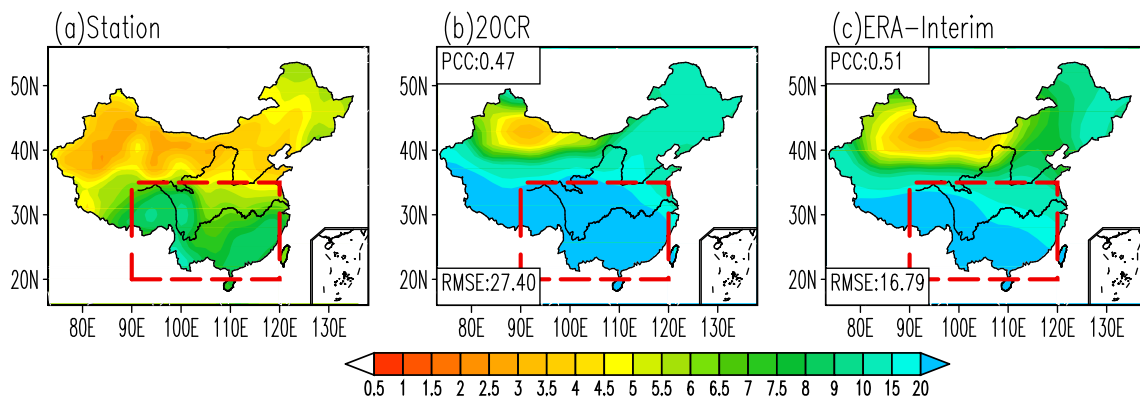


Fig. 8 Same as Fig. 6, but for the climatological annual mean (1979–2011) of CWD. The red dashed boxes indicate the southern part of China (90°–120° E, 20°–35° N)

5 The variation of persistent climate extremes response to the temperature variations

In the above, we evaluated the ability of two reanalysis datasets to depict persistent precipitation extremes and persistent temperature extremes, separately. As indicated in the introduction, the relationship between the precipitation (including precipitation extremes) and temperature (including global temperature and local temperature) is also important (Nicholls 2004). In this section, the relationship between the persistent

precipitation extremes and temperature variations has been examined.

On one hand, the global-mean surface temperature anomaly (GTemp) has been identified as the background temperature. Based on station data, the normalized CDD, CWD, Rx5d, and GTemp over eight sub-regions in 1979–2011 is calculated. The linear fitting is used to quantitatively diagnose the response of the persistent precipitation extremes against the temperature variations. Specifically, only the results with significance at the 90 % confidence level are shown in Fig. 11.

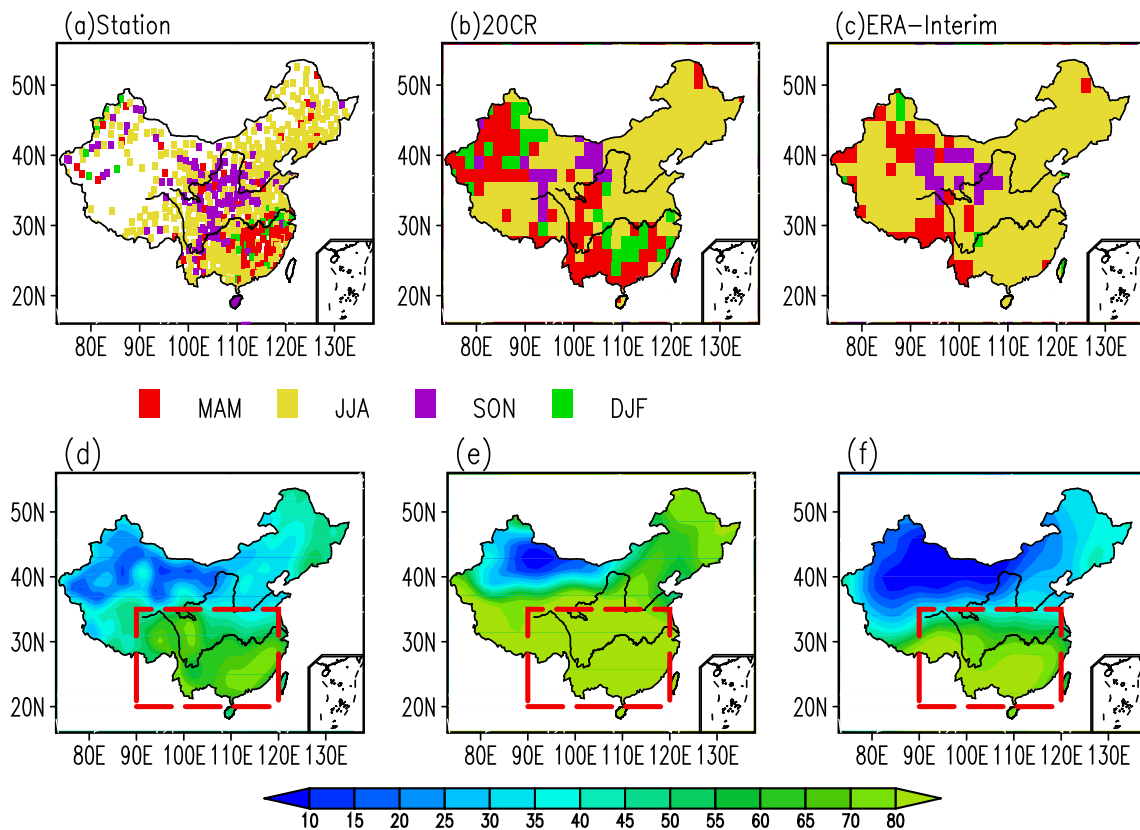


Fig. 9 The climatological (1979–2011) occurrence season of CWD (a–c) and the numbers of rain days during spring and summer (d–f) in station data (the left column), 20CR (the middle column) and ERA-Interim (the right column). The red dashed boxes in panels d–f indicate the southern part of China (90°–120° E, 20°–35° N)

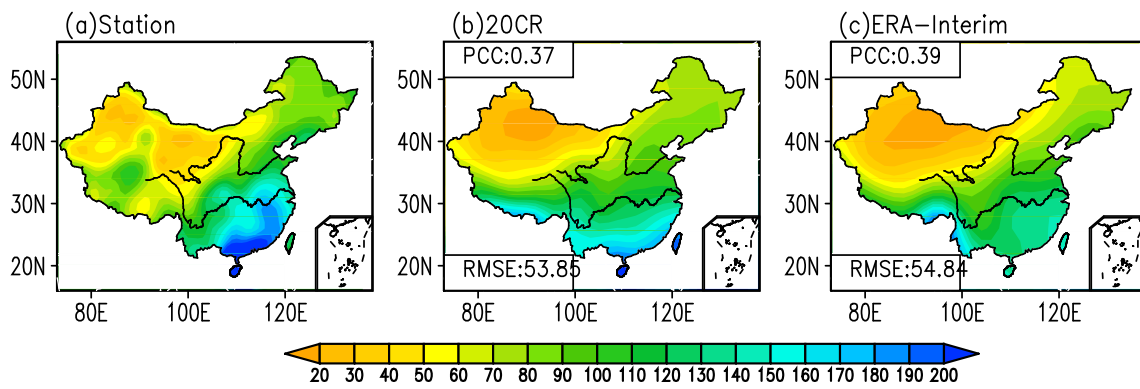


Fig. 10 Same as Fig. 6, but for the climatological annual mean (1979–2011) of Rx5d

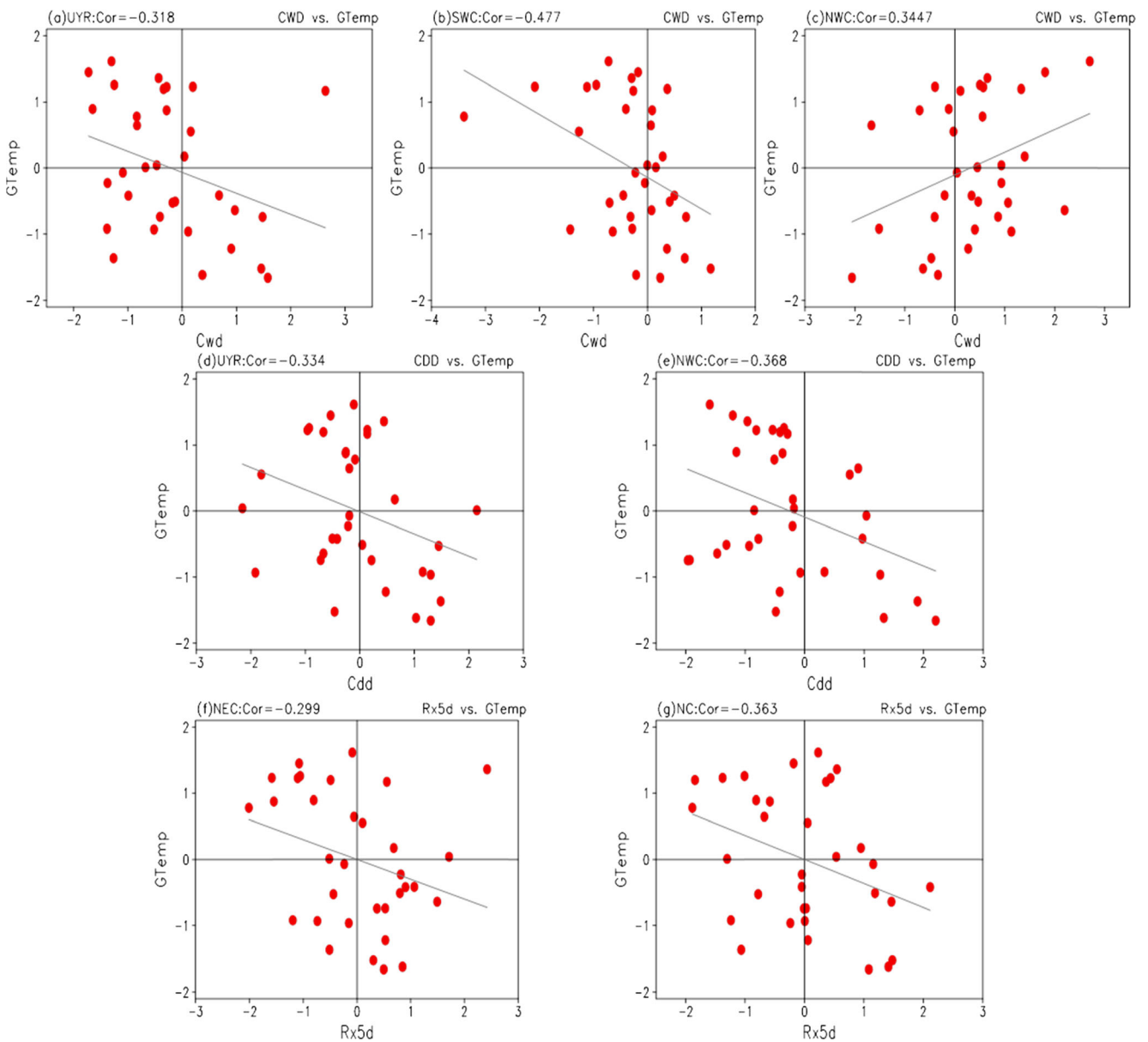


Fig. 11 Normalized annual CWD against normalized annual global temperature anomaly over UYR (a), SWC (b), and NWC (c), normalized annual CDD against normalized annual global temperature anomaly over UYR (d) and NWC (e), and normalized annual Rx5d

against normalized annual global temperature anomaly over NEC (f) and NC (g) in 1979–2011 from station data. The linear fitting line (sloping solid line in each figure) and the correlation coefficient (left title in each figure) are shown

Table 4 The correlation coefficients of linear fitting between CWD, CDD, Rx5d and global temperature variation over specific regions. Values with magnitude significant at the 90 % confidence level are in italics

Region	CWD vs. GTemp			CDD vs. GTemp		Rx5d vs. GTemp	
	UYR	SWC	NWC	UYR	NWC	NEC	NC
Station	<i>-0.32</i>	<i>-0.45</i>	<i>-0.35</i>	<i>-0.33</i>	<i>-0.37</i>	<i>-0.3</i>	<i>-0.36</i>
20CR	<i>-0.15</i>	0.11	<i>-0.16</i>	<i>-0.15</i>	<i>-0.16</i>	<i>-0.32</i>	<i>-0.18</i>
ERA-Interim	<i>0.36</i>	<i>-0.39</i>	<i>-0.12</i>	<i>-0.38</i>	<i>-0.16</i>	<i>-0.31</i>	0.01

It shows that significant negative correlations between CWD and GTemp mainly locate over UYR and SWC, while the positive correlations are over NWC (Fig. 11a–c). It suggests that associated with global warming, the longest persistent wet day has shortened over UYR and SWC and elongated over NWC. By comparison between the two reanalysis datasets, only significant negative between CWD and GTemp over SWC can be detected by the ERA-Interim (Table 4). For the relationship between CDD and GTemp, significant negative correlations exist over UYR and NWC (Fig. 11d–e). It suggests that associated with global warming, the maximum persistent dry days have shortened. For the relationship between Rx5d and GTemp, significant negative correlations lie over NEC and NC. It suggests reduced persistent precipitation intensity is associated with global warming. Both the two reanalysis datasets have the ability to detect the negative correlations between CDD and GTemp or between Rx5d and GTemp, particularly for the ERA-Interim (Table 4).

On the other hand, the relationship between the persistent temperature and persistent precipitation extremes has been analyzed, which represents the response of the precipitation extremes against the local temperature change. Since the two reanalysis datasets have better performances on the intensity indices of persistent temperature extremes (particular for the HWFM and CWFm), we chose HWFM and CWFm to identify the local temperature variations. Based on the normalized CDD and CWFm, CWD and HWFM, and Rx5d and CWFm in the period of 1979–2011, the linear fittings over significant regions are shown in Fig. 12. For the relationship between CDD and CWFm, significant negative correlations exist over NEC, NC, and UYR (Fig. 12a–c). It suggests that associated with the longer consecutive dry days, the larger magnitude of the longest cold spell extremes would exist over the northern part of China. However, the two reanalysis datasets cannot detect the relationship between the CDD and CWFm (Table 5). For the relationship between CWD and HWFM,

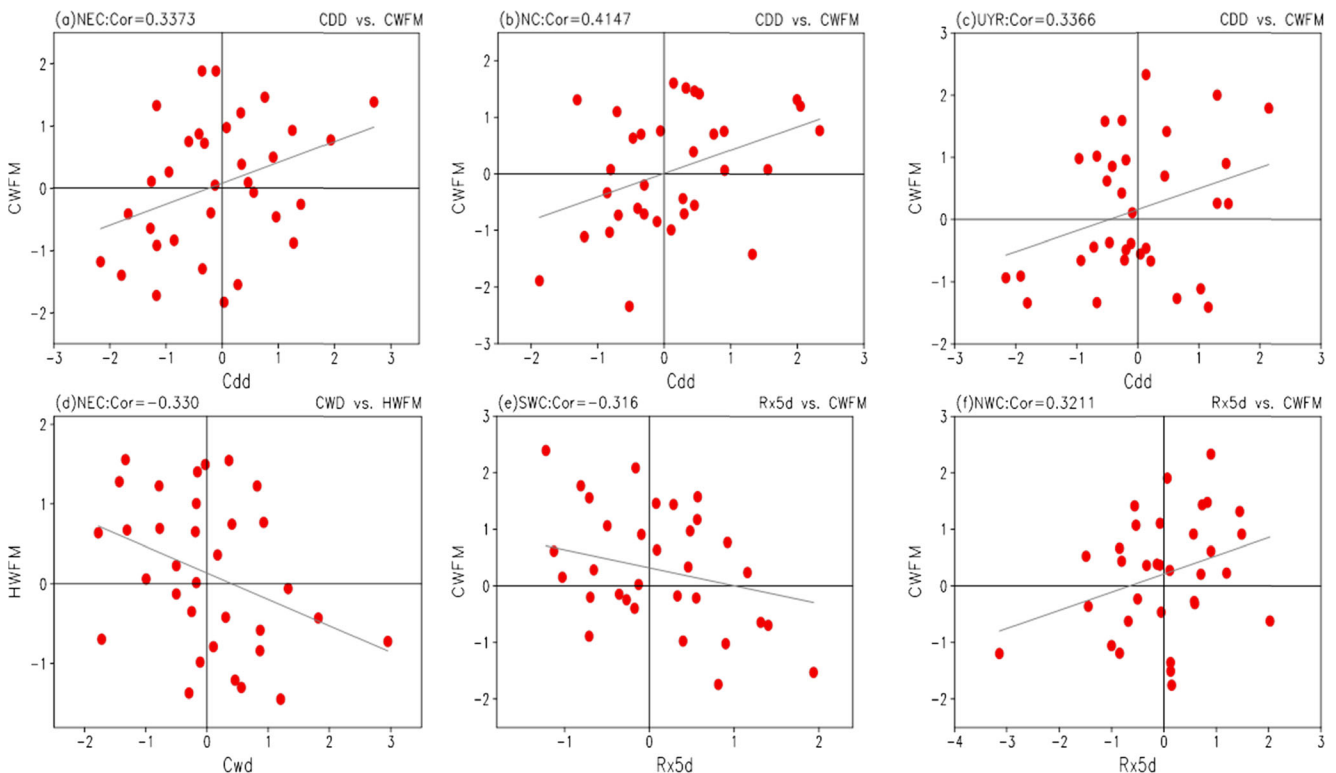


Fig. 12 Normalized annual CDD against normalized annual CWFm over NEC (a), NC (b) and UYR (c), normalized annual CWD against normalized HWFM over NEC (d), and normalized annual Rx5d against

normalized CWFm over SWC (e) and NWC (f) in 1979–2011 from station data. The linear fitting line (*sloping solid line in each figure*) and the correlation coefficient (*left title in each figure*) are shown

Table 5 The correlation coefficients of linear fitting between CWD, CDD, Rx5d and CWFM and HWFM over specific regions. Values with magnitude significant at the 90 % confidence level are in italics

Region	CDD vs. CWFM			CWD vs. HWFM		Rx5d vs. CWFM	
	NEC	NC	UYR	NEC	SWC	NWC	
Station	<i>0.34</i>	<i>0.41</i>	<i>0.34</i>	<i>-0.33</i>	<i>-0.32</i>	<i>0.32</i>	
20CR	0.18	0.26	0.01	<i>-0.38</i>	0.12	-0.07	
ERA-Interim	0.13	0.13	<i>0.3</i>	<i>-0.31</i>	0.25	0.19	

significant negative relationships lie over NEC. It indicates that associated with the longer consecutive wet days, the larger magnitude of the longest warm spell extremes may exist over NEC. Both the reanalysis datasets can detect the significant negative correlations between CWD and HWFM (Table 5). For the relationship between Rx5d and CWFM, significant negative (positive) correlations have been indicated over SWC (NWC). However, the two reanalysis datasets cannot detect the relationship (Table 5). In all, the ERA-Interim reanalysis has quite a better ability than the 20CR to identify the response of the persistent precipitation extremes against the temperature variations.

6 Conclusions and discussions

In this study, the performance of 20CR and ERA-Interim reanalysis datasets on depicting the persistent temperature and precipitation extremes has been evaluated during the period of 1979–2011. For the persistent temperature extremes, two reanalysis datasets have higher skill of depicting the intensity indices than depicting the frequency indices, with the lowest skills of depicting the percentile frequency indices (HWFI

and CWFI). Despite the regional differences, the two reanalysis datasets have the ability to detect that China has experienced significant increase of persistent warm extremes and decrease of the persistent cold extremes, particularly over the northern part of China. Generally, ERA-Interim quite reasonably reproduces the climatology and tendency of persistent warm extremes, while the 20CR has quite good skill for the persistent cold extremes.

The ERA-Interim can well capture the CDD and CWD over Eastern and Northwestern China, respectively. However, the two reanalysis datasets have largely underestimated (overestimated) the CDD (CWD) over the northern (southern) part of China. This is partially due to the incorrectly reproduced occurrence season and great underestimation (overestimation) of the dry days (rain days). The two reanalysis datasets also have the ability to capture the climatological Rx5d, particularly over the northern part of China. To sum up, the two reanalysis datasets have good skills to capture the persistent temperature extremes, while large uncertainties lie in depicting the persistent precipitation extremes. These are also consistent with Yin et al.’s (2015) latest study.

The variation of persistent precipitation extremes responding to the temperature variation has been further examined. Responding to the background temperature variation, the longest persistent wet day has prolonged over UYR and SWC, while shortened over NWC. For the relationship between CDD and GTemp, significant negative relationships exist over UYR and NWC. The Rx5d significantly decreases in a warm climate over NEC and NC. In comparison, the ERA-Interim has better ability to capture the relationship than the 20CR. For the local temperature variation, both the two reanalysis datasets have good ability to detect the negative correlations between CWD and HWFM over NEC.

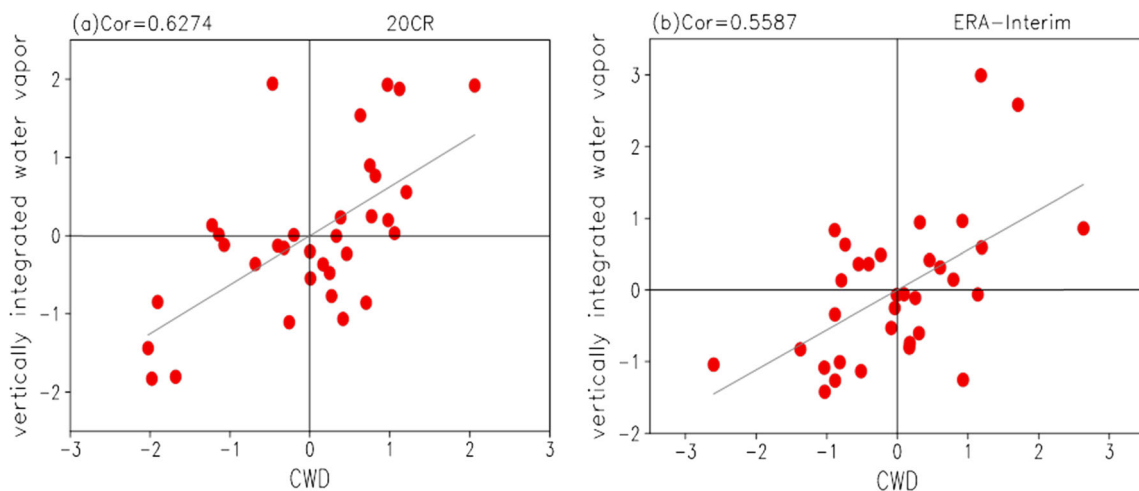


Fig. 13 Normalized annual CWD against normalized annual vertically integrated water vapor over northern part of China (including NEC and NC) in 1979–2011 from 20CR (a) and ERA-Interim (b). The linear fitting

line (sloping solid line in each figure) and the correlation coefficient (left title in each figure) are shown

Associated with the long consecutive dry days, the large magnitude of the longest cold spell extremes would exist over the northern part of China. However, the two reanalysis datasets cannot capture the relationship between the CDD and CWF. Either they cannot capture the positive (negative) correlations between Rx5d and CWF over SWC (NWC).

As indicated in the relationship between precipitation and temperature extremes, the northern part of China may be a very sensitive region. Focused on Beijing, a megacity in North China, Chen and Lu (2014) has linked the extreme heat and water vapor. They indicated that under a suitable large-scale circulation, reduced water vapor flux may enhance the solar radiation at the surface, and therefore provides a benefit condition for the temperature extremes. This is in agreement with our results based on the two reanalysis datasets about the negative correlations between CWD and HWFM over the northern part of China (including NEC and NC), since significant positive correlations link the CWD and vertically integrated water vapor (Fig. 13). Moreover, Chen and Lu (2015) and Lu and Chen (2016) revealed that the extreme heat over northeastern China can be classified as typical extratropical pattern and emphasize the role of the anticyclone. The anticyclone may influence the water vapor transportation and therefore affect the precipitation. However, they focused on single-day extreme, and the mechanism for the linkage between persistent temperature and precipitation extremes should need a further analysis.

Acknowledgments This study is jointly sponsored by the National Key Research and Development Program of China (Grant Nos. 2016YFA0600701 and 2016YFA0601504), the National Natural Science Foundation of China (Grant Nos. 41575071 and 51190091), Key Laboratory of Meteorological Disaster of Ministry of Education, Nanjing University of Information Science and Technology (KLME1502), and the Jiangsu Collaborative Innovation Center for Climate Change.

References

- Alexander LV, Zhang X, Peterson TC, et al. (2006) Global observed changes in daily climate extremes of temperature and precipitation. *J Geophys Res* 111:D05109. doi:10.1029/2005JD006290
- Allan RP, Soden BJ (2008) Atmospheric warming and the amplification of precipitation extremes. *Science* 321:1481–1484. doi:10.1126/science.1160787
- Bao X, Zhang F (2013) Evaluation of NCEP–CFSR, NCEP–NCAR, ERA-interim, and ERA-40 reanalysis datasets against independent sounding observations over the Tibetan plateau. *J Clim* 26:206–214. doi:10.1175/JCLI-D-12-00056.1
- Berg P, Moseley C, Haerter JO (2013) Strong increase in convective precipitation in response to higher temperatures. *Nat Geosci* 6:181–185. doi:10.1038/ngeo1731
- Bosilovich MG, Chen J, Robertson FR, Adler RF (2008) Evaluation of global precipitation in reanalyses. *J Appl Meteorol Climatol* 47:2279–2299. doi:10.1175/2008JAMC1921.1
- Chen R, Lu R (2014) Large-scale circulation anomalies associated with “tropical night” weather in Beijing, China. *Int J Climatol* 34:1980–1989. doi:10.1002/joc.3815
- Chen R, Lu R (2015) Comparisons of the circulation anomalies associated with extreme heat in different regions of eastern China. *J Clim*. doi:10.1175/JCLI-D-14-00818.1
- Chen Y, Zhai P (2015) Mechanisms for concurrent low-latitude circulation anomalies responsible for persistent extreme precipitation in the Yangtze River valley. *Clim Dyn*. doi:10.1007/s00382-015-2885-6
- Compo GP, Whitaker JS, Sardeshmukh PD, et al. (2011) The twentieth century reanalysis project. *Q J R Meteorol Soc* 137:1–28. doi:10.1002/qj.776
- Dee DP, Uppala SM, Simmons AJ, et al. (2011) The ERA-interim reanalysis: configuration and performance of the data assimilation system. *Q J R Meteorol Soc* 137:553–597. doi:10.1002/qj.828
- Donat MG, Alexander LV, Yang H, et al. (2013) Global land-based datasets for monitoring climatic extremes. *Bull Am Meteorol Soc* 94:997–1006. doi:10.1175/BAMS-D-12-00109.1
- Donat MG, Sillmann J, Wild S, et al. (2014) Consistency of temperature and precipitation extremes across various global gridded in situ and reanalysis datasets. *J Clim*. doi:10.1175/JCLI-D-13-00405.1
- Frich P, Alexander LV, Della-Marta P, et al. (2002) Observed coherent changes in climatic extremes during the second half of the twentieth century. *Clim Res* 19:193–212. doi:10.3354/cr019193
- Hodges KI, Lee RW, Bengtsson L (2011) A comparison of extratropical cyclones in recent reanalyses ERA-interim, NASA MERRA, NCEP CFSR, and JRA-25. *J Clim* 24:4888–4906. doi:10.1175/2011JCLI4097.1
- Huang D, Qian Y, Zhu J (2010) Trends of temperature extremes in China and their relationship with global temperature anomalies. *Adv Atmos Sci* 27:937–946. doi:10.1007/s00376-009-9085-4.1
- Huang D, Zhu J, Zhang Y, et al. (2016) Assessment of summer monsoon precipitation derived from five reanalysis datasets over East Asia. *Q J R Meteorol Soc* 142:108–119. doi:10.1002/qj.2634
- Ivancic TJ, Shaw SB (2016) A U.S. based analysis of the ability of the clausius-clapeyron relationship to explain changes in extreme rainfall with changing temperature. *J Geophys Res Atmos*. doi:10.1002/2015JD024288
- Kendall M (1975) Rank correlation methods, 4th edn. Charles Griffin, London
- Lenderink G, van Meijgaard E (2008) Increase in hourly precipitation extremes beyond expectations from temperature changes. *Nat Geosci* 1:511–514. doi:10.1038/ngeo262
- Lenderink G, van Meijgaard E (2010) Linking increases in hourly precipitation extremes to atmospheric temperature and moisture changes. *Environ Res Lett* 5:025208. doi:10.1088/1748-9326/5/2/025208
- Li G, Harrison SP, Bartlein PJ, et al. (2013) Precipitation scaling with temperature in warm and cold climates: an analysis of CMIP5 simulations. *Geophys Res Lett* 40:4018–4024. doi:10.1002/grl.50730
- Liao Z, Zhang Y (2013) Concurrent variation between the east Asian subtropical jet and polar front jet during persistent snowstorm period in 2008 winter over southern China. *J Geophys Res Atmos* 118:6360–6373. doi:10.1002/jgrd.50558
- Lin R, Zhou T, Qian Y (2014) Evaluation of global monsoon precipitation changes based on five reanalysis datasets. *J Clim* 27:1271–1289. doi:10.1175/JCLI-D-13-00215.1
- Lu R, Chen R (2016) A review of recent studies on extreme heat in China. *Atmos Ocean Sci Lett* 9:114–121. doi:10.1080/16742834.2016.1133071
- Ma L, Zhang T, Li Q, et al. (2008) Evaluation of ERA-40, NCEP-1, and NCEP-2 reanalysis air temperatures with ground-based measurements in China. *J Geophys Res Atmos* 113:1–15. doi:10.1029/2007JD009549
- Ma L, Zhang T, Frauenfeld OW, et al. (2009) Evaluation of precipitation from the ERA-40, NCEP-1, and NCEP-2 reanalyses and CMAP-1,

- CMAP-2, and GPCP-2 with ground-based measurements in China. *J Geophys Res* 114:D09105. doi:[10.1029/2008JD011178](https://doi.org/10.1029/2008JD011178)
- Mann H (1945) Non-parametric tests against trend. *Econometrica* 13: 245–259
- Morice CP, Kennedy JJ, Rayner NA, Jones PD (2012) Quantifying uncertainties in global and regional temperature change using an ensemble of observational estimates: the HadCRUT4 data set. *J Geophys Res* 117:D08101. doi:[10.1029/2011JD017187](https://doi.org/10.1029/2011JD017187)
- Nicholls N (2004) The changing nature of Australian droughts. *Clim Chang* 63:323–336
- O’Gorman PA, Schneider T (2009) The physical basis for increases in precipitation extremes in simulations of 21st-century climate change. *Proc Natl Acad Sci U S A* 106:14773–14777. doi:[10.1073/pnas.0907610106](https://doi.org/10.1073/pnas.0907610106)
- Smith SR, Legler DM, Verzone KV (2001) Quantifying uncertainties in NCEP reanalyses using high-quality research vessel observations. *J Clim* 14:4062–4072
- Sun Y, Zhang X, Zwiers FW, et al. (2014) Rapid increase in the risk of extreme summer heat in eastern China. *Nat Clim Chang* 4:1082–1085. doi:[10.1038/nclimate2410](https://doi.org/10.1038/nclimate2410)
- Trenberth K, Shea D (2005) Relationships between precipitation and surface temperature. *Geophys Res Lett.* doi:[10.1029/2005GL022760](https://doi.org/10.1029/2005GL022760)
- Trenberth KE, Stepaniak DP, Hurrell JW (2001) Quality of reanalyses in the tropics. *J Clim* 14:1499–1510
- Westra S, Fowler HJ, Evans JP, et al. (2014) Future changes to the intensity and frequency of short-duration extreme rainfall. *Rev Geophys* 52:522–555. doi:[10.1002/2014RG000464](https://doi.org/10.1002/2014RG000464)
- Williams IN, Torn MS, Riley WJ, Wehner MF (2014) Impacts of climate extremes on gross primary production under global warming. *Environ Res Lett* 9:094011. doi:[10.1088/1748-9326/9/9/094011](https://doi.org/10.1088/1748-9326/9/9/094011)
- Wu FT, Fu CB (2013) Change of precipitation intensity spectra at different spatial scales under warming conditions. *Chinese Sci Bull* 58: 1385–1394. doi:[10.1007/s11434-013-5699-0](https://doi.org/10.1007/s11434-013-5699-0)
- Ye H, Fetzer EJ, Behrangi A, et al. (2016) Increasing daily precipitation intensity associated with warmer air temperatures over northern Eurasia. *J Clim* 29:623–636. doi:[10.1175/JCLI-D-14-00771.1](https://doi.org/10.1175/JCLI-D-14-00771.1)
- Yin H, Donat MG, Alexander LV, Sun Y (2015) Multi-dataset comparison of gridded observed temperature and precipitation extremes over China. *Int J Climatol* 35:2809–2827. doi:[10.1002/joc.4174](https://doi.org/10.1002/joc.4174)
- You Q, Fraedrich K, Min J, et al. (2013) Can temperature extremes in China be calculated from reanalysis? *Glob Planet Change* 111:268–279
- Zhao T, Fu C (2006a) Preliminary comparison and analysis between ERA-40, NCEP-2 reanalysis and observations over China. *Clim Environ Res (in Chinese)* 11:14–32
- Zhao T, Fu C (2006b) Comparison of products from ERA-40, NCEP-2, and CRU with station data for summer precipitation over China. *Adv Atmos Sci* 23:593–604